Rodríguez-Sierra, J.C.; Soria, A.

TWO MODELS OF ELECTRICAL IMPEDANCE FOR ELECTRODES WITH TAP WATER
AND THEIR CAPABILITY TO RECORD GAS VOLUME FRACTION

TWO MODELS OF ELECTRICAL IMPEDANCE FOR ELECTRODES WITH TAP WATER AND THEIR CAPABILITY TO RECORD GAS VOLUME FRACTION

DOS MODELOS DE IMPEDANCIA ELÉCTRICA PARA ELECTRODOS CON AGUA POTABLE Y SU CAPACIDAD DE REPRESENTAR LA FRACCIÓN VOLUMEN DE GAS

J.C. Rodríguez-Sierra and A. Soria*

Departamento de Ingeniería de Procesos e Hidráulica. División CBI, Universidad Autónoma Metropolitana-Iztapalapa. San Rafael Atlixco No. 186 Col. Vicentina, CP 09340 Cd. de México, México.

Abstract

Bubble columns are devices for simultaneous two-phase or three-phase flows. Phase interactions produce several flow patterns where the void fraction is an important variable involved in the behavior and fundamental in flow pattern transitions. Electrical impedance sensors (EIS) determine void fraction and perform as fast response, passive elements, exhibiting resistive, capacitive and inductive behaviors highly dependent upon the excitation frequency. A simple electrical model frequently used is a set of a resistance and a capacitor connected in parallel. Same elements can also be arranged in series, as we do here. We identify three behaviors in the series and parallel arrangements, as well as in the experimental data. While the ones of the series arrangement are coincident with experimental data, the ones of the parallel model are only partially coincident at high frequencies. Moreover, while the parallel model is insensitive to changes in gas volume fraction in the resistive range, the series model presents sensitivity to changes in the gas volume fraction. Therefore, on these grounds the series arrangement exhibits a better performance than the parallel model.

Keywords: electrical impedance, series model, parallel model, tap-water model, void fraction, air-water flow, bubble column.

Resumen

Las columnas de burbujeo son dispositivos para el flujo simultáneo de dos o tres fases. La interacción entre fases produce varios patrones de flujo, donde la fracción volumen de gas es una variable importante implicada en el comportamiento de los patrones de flujo y es fundamental en sus transiciones. Los sensores de impedancia eléctrica (SIE) determinan la fracción de vacío y se desempeñan con respuesta rápida, elementos pasivos que despliegan comportamientos resistivo, capacitivo e inductivo ampliamente dependientes de la frecuencia de excitación. Un modelo eléctrico sencillo que se ha usado con frecuencia es un conjunto de una resistencia y un condensador en paralelo. Los mismos elementos pueden ser dispuestos en serie, como lo hacemos aquí. Identificamos tres comportamientos de los arreglos en serie y en paralelo, así como de los datos experimentales. Los del arreglo en serie coinciden con los de los datos experimentales, en tanto que los del modelo en paralelo sólo parcialmente para altas frecuencias. Además, mientras el modelo en paralelo es insensible a los cambios de fracción volumen de gas en el régimen resistivo, el modelo en serie presenta sensibilidad a los cambios en la fracción volumen de gas. Sobre estas bases, el arreglo en serie presenta un mejor desempeño que el modelo en paralelo.

Palabras clave: impedancia eléctrica, modelo en serie, modelo en paralelo, modelo del agua, fracción vacío, flujo aire-agua, columna de burbujeo.

1 Introduction

Dispersed multiphase flows play an important role in the process industries. Among these flows, those with two or three phases are the most frequent. Gas-liquid flows inside pipes are used for many industrial applications (Falcone, 2009a) spanning from bubble columns, where the liquid is the continuous phase and the gas is thinly dispersed in small bubbles, to misty or fog flows. In these flows the gas is the continuous phase and the liquid is dispersed in tiny drops or fog. A third phase can also be present in a bubble column as a dispersed phase; thus, a solid powder or swarms of solid particles or pellets

Correspondingn author. E-mail: asor@xanum.uam.mx
Tel. 55-5804-4648, Fax 55-5804-4900

can configure the third phase, as in waste water treatment columns or in three-phase fluidized bed chemical reactors. There is interest on studying the occurrence of several geometrical configurations of the dispersed phases, called flow patterns, in a bubble column, both for design and for operation purposes. Some parameters, such as the physical properties of the materials, their mass flow rates, their volume fractions, the column length and diameter, as well as its tilting, determine not only the flow patterns but also the transitions between them (Taitel *et al.*, 1980; Spedding and Nguyen, 1980; Li *et al.*, 2016). Some methods have been proposed to classify flow patterns using characteristic variables such as void fraction fluctuations or differential pressure, which are supposed to reflect the flow configuration (Song *et al.* 1995; Costigan and Whalley 1997; Cheng *et al.* 2002; Rodríguez, 2006). Transitions between flow patterns are complex phenomena closely related to interactions between bubbles and fluid, where the void fraction (the gas volume fraction) becomes a very important dynamic variable (Zenit and Hunt, 2000; Banasiak *et al.*, 2014) whose stability analysis can enlighten the occurrence of the regime transitions (Soria and Salinas-Rodríguez, 2013; Sánchez-López *et al.* 2011; Cheng *et al.* 2002).

Various definitions are used for specifying the void fraction: local-instantaneous, time averaged, cross-sectional and volumetric among others. The volumetric void fraction is based on the relative volume occupied by the respective phase. In this study, the local volume fraction of a given fluid, at a given point **x** in a two-phase mixture, is defined as the volume occupied by the fluid in a representative elementary volume (REV), as a fraction of the whole REV. The centroid of the REV is placed at point **x**. In particular, the REV in the experimental EIS (*c. fr.* Fig. 3) is coincident with the slice sensed by the electrodes. There are some volume fraction experimental measurement techniques (Prasser, 2007; Falcone, 2009b; Coutinho *et al.* 2014) such as the acoustic attenuation, microwave attenuation, ultrasound, tomography, wire-mesh and electrical impedance. This last technique is the simplest and probably the cheapest of all techniques (Rocha, 2008) and allows measurements of the void fraction with resolution times of 10^{-3} *s* and smaller.

The electrical impedance is frequently used for the characterization of components, systems, and materials (Martínez Gómez and Soria, 2003). Electrical impedance is expressed as a complex number, whose real part is the resistance and whose imaginary part is the reactance. Impedance multiphase flow measurements can be divided in two broad topics: the impedance intrusive device, with electrodes separated by few millimeters, commonly mounted on an immersion probe and used for local measurements of the void fraction and the impedance not-intrusive device, flushed to the inside wall or at the outside wall of the pipe, used for the whole cross sectional void fraction (Micaelli, 1982; Bernier, 1982; Tournaire, 1986, 1987).

Studies on air-water flows using electrical impedance are usually performed to measure impedance as a function of the frequency and the voltage or the intensity of the applied current (Ko *et al.*, 2015). To measure the void fraction, sensors are made with electrodes or sets of electrodes. Each electrode embraces a detection volume crossed by the air-water flow. Volumetric fractions and interfacial areas are the more important geometrical parameters in multiphase flows. In general, both are independent parameters (Soria and de Lasa, 1992). Bernier (1982), following Maxwell, establishes relationships between electrical parameters and the volume fraction of the conductive phase. Thus, relationships with interfacial areas should be established specifically, probably for different arrangements of small electrodes and taking care about the geometrical shapes, as Maxwell theory is being applied.

Sensors with specific characteristics of electrodes (geometry, electrode size, electrode shape), for several operating conditions (excitation frequency, conductance method or capacitance method) have been developed (Bernier, 1982; George *et al.*, 2001; Devia and Fossa, 2003, Yang *et al.*, 2003). Tournaire (1986) defined the geometry of the probe by the width and the number of electrodes.

The air-tap water two-phase system, flowing through the detection zone, is usually modeled by a capacitor and a resistance. The elementary electrical model of the impedance sensor and the measuring system that operates without electrolysis near electrode surfaces can be compared to a RC circuit (Rocha, 2008; Mansfeld *et al.*, 1993). The analysis of a RC model shows a simple way to associate the overall two-phase mixture behavior with their corresponding arranged electrical elements. The parallel arrangement seems to have been frequently assumed without experimental verification (dos Reis and da Silva, 2014; Micaelli, 1982; Bernier, 1982; Tournaire, 1986, 1987, Sainz-Jabardo and Bouré, 1988; Kytömaa and Brennen, 1988; Jaworek *et al.*, 2004; Tri, 2005; Wu *et al.*, 2015), series arrangement

does not seem to have been reported. This kind of models is used for the evaluation of the behavior of the electrical impedance sensor in the frequency domain, to determine the operation mode, *i.e.* the capacitive mode or the resistive mode.

The purpose of this communication is to show that the series model of the basic capacitor/resistance arrangement of electrodes in the air-tap water two-phase systems in a bubble column fits the experimental data in a wider interval of excitation frequencies than the parallel model, including the low range frequencies, where electrode capacitive behavior is known to occur. It is also our purpose to show that the series model provides a simple, yet meaningful piece of information for further modeling development, since it discriminates between different volume fraction values in the resistive range.

2 Transfer functions of two-phase system

A voltage divider is set with respect to ground by connecting two electrical impedances in series, as shown in Fig. 1. The input voltage is applied across the series impedances and the output is the voltage across Z_2 or Z_1. The impedances Z_1 and Z_2 may be arranged in any combination of elements such as resistors, inductors, and capacitors. Table 1 shows the impedance elements.

Applying Ohm's law, the relationship between input voltage, V_{in}, and the output voltage, V_1 or V_2, can be found and the transfer function or divider's voltage ratio for this circuit is:

$$H_i = \frac{V_i}{V_{in}} = \frac{Z_i}{Z_1 + Z_2} \tag{1}$$

where, the subscript "*i*" denotes 1 or 2, according to the point of measure.

Table 1. Impedances of passive elements.

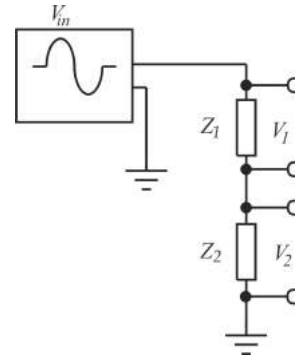| Element	Impedance
R(Resistor)	$Z = R_z$
C(Capacitor)	$Z = \frac{1}{j\omega C_z}$
L(Inductor)	$Z = j\omega L_z$

Fig. 1. Voltage divider with two components arranged in series.

We analyzed the case where Z_1 is purely resistive and Z_2 is the multiphase system composed by both resistive and capacitive elements (see Fig. 2), therefore Z_2 is a function of ωj. Substituting $Z_1 = R$ and $Z_2 = Z(\omega j)$ the previous expression gives:

$$H_1(\omega j) = \frac{V_1}{V_{in}} = \frac{R}{R + Z(\omega j)} \tag{2}$$

and

$$H_2(\omega j) = \frac{V_2}{V_{in}} = \frac{Z(\omega j)}{R + Z(\omega j)} \tag{3}$$

where, $H_1(\omega j)$ is the transfer function according to R and $H_2(\omega j)$ is the transfer function according to $Z(\omega j)$.

The multiphase system is represented by $Z(\omega j)$, but the configuration of the arrangement between resistive and capacitive parts is not yet determined. Because of the electrical properties of tap-water, the impedance of the two-phase system is made up by a capacitance C_{TP} and a resistance R_{TP} distributed over the detection volume, if volume is defined by the lines of an electric field associated to the electrode system. The two possible configurations of $Z(\omega j)$ to be tested are: (1) the components connected in series $Z_s(\omega j)$ (Fig. 2(a)) and (2) the components connected in parallel $Z_p(\omega j)$ (Fig. 2(b)). Here the subscripts *s* and *p* stand for the series and parallel arrangements, respectively. These impedance expressions for the series and parallel RC circuits are:

$$Z_s(\omega j) = R_{TP} + \frac{1}{C_{TP}\omega j} \tag{4}$$

and

$$Z_p(\omega j) = \frac{R_{TP}}{1 + C_{TP}R_{TP}\omega j} \tag{5}$$

The relationship between the impedance of water and the impedance of the two-phase flow system is

(a) Impedance $Z_s(\omega j)$ with components connected in series

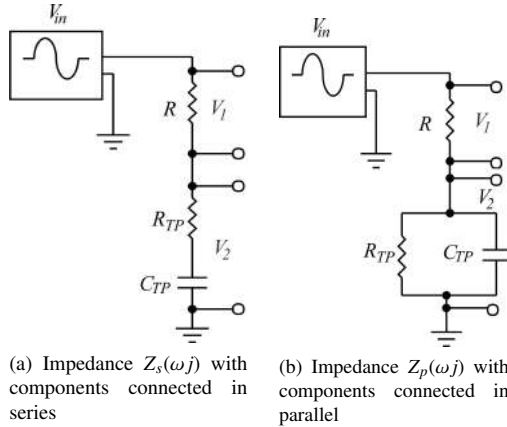(b) Impedance $Z_p(\omega j)$ with components connected in parallel

Fig. 2. Resistor/impedance arrangements in voltage divider.

developed by Bernier (1982) after Maxwell. The two-phase resistance R_{TP} and the two-phase capacitance C_{TP} are given by:

$$R_{TP} = \frac{R_z}{\left(1 - \frac{3\alpha}{2+\alpha}\right)} \quad (6)$$

and

$$C_{TP} = C_z\left(1 - \frac{3\alpha}{2+\alpha}\right) \quad (7)$$

where R_z and C_z are resistance and capacitance values for water without bubbles ($\alpha = 0$) to be found by fitting experimental points.

The transfer functions can now be expressed for models in series and in parallel according to the detection points 1 and 2. Substituting Eq. (4) and Eq. (5) into Eq. (2), we get, at the detection point 1, for series model:

$$H_1^s(j\omega) = \frac{j\omega RC_{TP}}{1 + (R + R_{TP})C_{TP}j\omega} \quad (8)$$

and for parallel model

$$H_1^p(j\omega) = \frac{R + RR_{TP}C_{TP}j\omega}{R + R_{TP} + RR_{TP}C_{TP}j\omega}. \quad (9)$$

Finding their modulus, the previous expressions give:

$$|H_1^s(j\omega)| = \left|\frac{j\omega RC_{TP}}{1 + (R + R_{TP})C_{TP}j\omega}\right|$$
$$= \frac{RC_{TP}\omega}{\sqrt{[\omega(R + R_{TP})C_{TP}]^2 + 1}} \quad (10)$$

and

$$|H_1^p(j\omega)| = \left|\frac{R + RR_{TP}C_{TP}j\omega}{R + R_{TP} + RR_{TP}C_{TP}j\omega}\right|$$
$$= \frac{\sqrt{[\omega RR_{TP}C_{TP}]^2 + R^2}}{\sqrt{[\omega RR_{TP}C_{TP}]^2 + [R + R_{TP}]^2}} \quad (11)$$

and similarly, for point 2:

$$|H_2^s(j\omega)| = \left|\frac{1 + j\omega R_{TP}C_{TP}}{j\omega(R + R_{TP})C_{TP} + 1}\right|$$
$$= \frac{[\omega R_{TP}C_{TP}]^2 + 1}{[\omega(R + R_{TP})C_{TP}]^2 + 1} \quad (12)$$

and

$$|H_2^p(j\omega)| = \left|\frac{R_{TP}}{R + R_{TP} + R_{TP}C_{TP}\omega j}\right|$$
$$= \frac{R_{TP}}{\sqrt{[\omega RR_{TP}C_{TP}]^2 + [R + R_{TP}]^2}} \quad (13)$$

Now the frequency response for each detection point can be plotted if the values of R_z, C_z and α are known.

3 Experimental technique

3.1 Experimental facility set-up

Figure 3 is a schematics of the facility, as designed for this study. This consists of a function generator and a resistance, the test section, and an oscilloscope. The test section used in the experiments is a cylindrical pipe made of transparent Plexiglas®with an inside diameter of $0.053\,m$ and a height of about $0.5\,m$. The test section is filled with tap water at ambient pressure
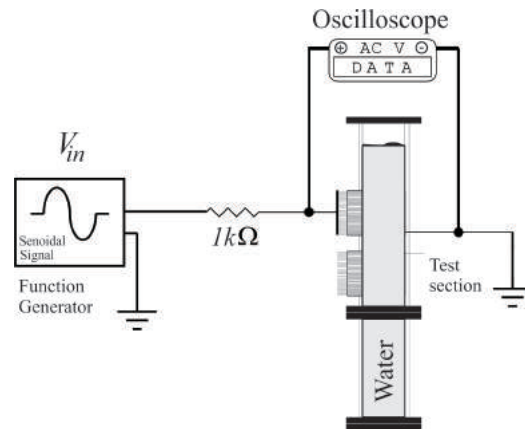

Fig. 3. Schematics of the experimental facility.

and temperature. The EIS has two sections of stainless steel plates. Steel plates are assembled, alternating with insulator plates 0.5 *mm* thick. Each electrode is composed of an active pole, made up by a selected number of metal plates, diametrically opposed to a common pole in each section and spanning 90 degree arcs on the circumference of the pipe, as can be observed in Fig. 3. Each section has 50 metal plates flush mounted to the inner wall, with 1 *mm* axial length. The opposed common pole in each section is 75 *mm* in axial length. Fig. 3 shows the electrode configuration.

3.2 Experimental procedure

To generate a single electrode, all the metal plates are connected to a single cable, thus we get the maximum size electrode. A sinusoidal a.c. signal is selected to avoid polarization and reaction in the electrodes (d.c.=0 volt) and a 5-volt potential peak to peak is applied across the 1 $k\Omega$ resistance and the EIS. This signal is provided by the function generator Insteck (GFG-3015), where the frequency is varied at four points per decade in the range of 0.1 *Hz* to 1 *MHz*; this is 1, 2.5, 5, 7.5, 10, 25, 50, 75, 100, *Hz*..., 1 *MHz*. The experimental transfer function can be obtained by measuring the input voltage V_{in} and the output voltage V_1 or V_2, for each one of the selected points, with the oscilloscope (Tektronix TDS 1002) and replacing the experimental values in Eq. (2) or (3) according to the case.

4 Results and discussion

4.1 General trends of models behavior

The transfer functions show that there are three possible behaviors: the capacitive behavior, the inductive behavior and the resistive behavior. In practical terms, the capacitive behavior is identified by the negative slope while the resistive behavior is identified by the zero slope and the inductive behavior is associated to a positive slope.

In order to plot the frequency response of the series and parallel models obtained in Section 2, we have to set the resistance R_{TP} and the capacitance C_{TP} of the system, according to Eq. (6) and Eq. (7). This requires the knowledge of R_z and C_z, the resistance and the capacitance of tap water without bubbles ($\alpha = 0$). An first adjustment of both parameters gave us the couple of optimized values: $C_z = 250 \mu F$ and $R_z = 95 \Omega$, these values were obtained by fitting the experimental data

using the series model, this will be discussed in the next sections. The optimization is performed using least squares in two stages. In the first stage optimal value of R_z was found only in the resistive interval, this step is justified by the specific knowledge that the transfer function is a constant in this interval, finding directly the value of R_z. In the second stage the value of the capacitance C_z was found by least squares.

In Fig. 4(a) the frequency response of both models, in a linear plot, according to detection point 1 is depicted. The $H_s(\alpha = 0)$ plot shows that the series system has an inductive behavior at frequencies between 0.1 and 1 *Hz*, whereas above 1 *kHz* it keeps a resistive behavior. The $H_p(\alpha = 0)$ plot shows that the parallel model has two resistive behaviors at low and high frequencies, whereas, in the middle, an inductive behavior about 1 to 100 *Hz* is apparent. Same frequency response is shown in decibels (*dB*) in Fig. 4(b). It is apparent that at small frequencies (1) the curvature of series model is smoother than the curvature in linear scale and (2) The two horizontal lines of the parallel model are closer to each other as well as very close to zero.

In Fig. 5(a) the frequency response of models according to detection point 2 is depicted in linear scale. The $H_s(\alpha = 0)$ linear plot shows that the series system has a resistive behavior above 1 *kHz*, while a capacitive behavior about 0.3 *Hz* to 3 *Hz* is apparent. In addition, the $H_p(\alpha = 0)$ linear plot for the parallel system presents a behavior with a resistive low frequency range, below 1 *Hz* and a second resistive-like range above 1 *kHz*, as well as a capacitive zone between them. The second resistive-like range is seen as a horizontal line at high frequencies and was firstly associated to a resistive behavior. However, when the magnitude plot was expressed in *dB*, see Fig. 5(b), the magnitude of the parallel model could be appreciated to be continuously decreasing, indicating a capacitive behavior. Nevertheless, the gain values are so small that the significance of this behavior could be confusing. This observation warns us to take advantage of the logarithmic scale representation.

4.2 Tap water measurements and modelling

Figs. 4 and 5 also show experimental data for tap water. It is observed that data hold a definite resistive pattern above 1 *kHz* of excitation frequency. This horizontal pattern is well fitted by the series model, both in detection point 1 (see Fig. 4) and in detection
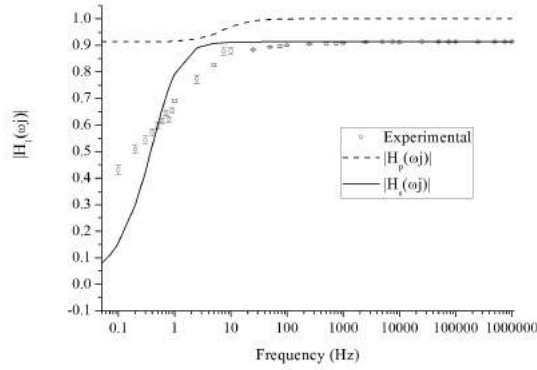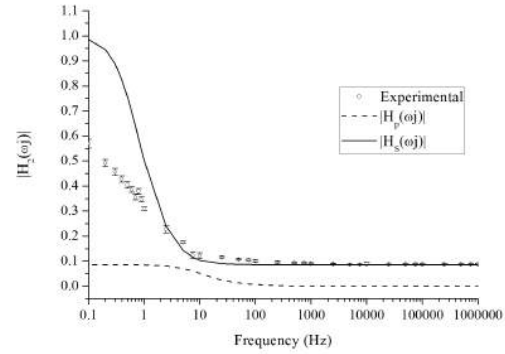
(a) Linear scale plot.
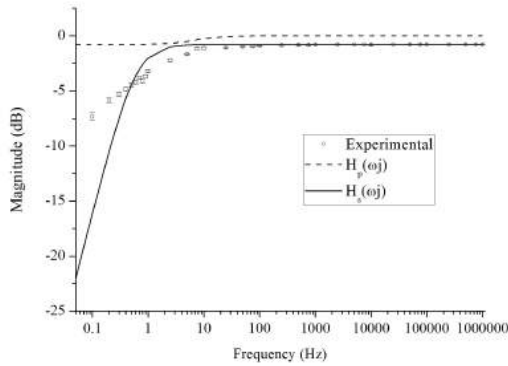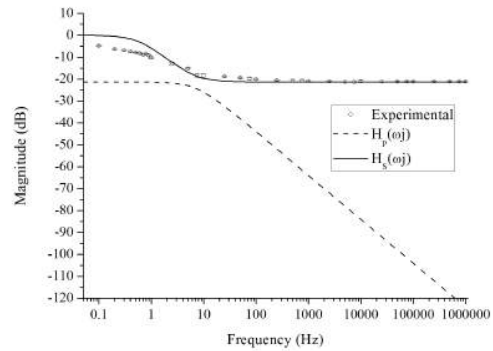

(b) Decibel (dB) scale plot.

Fig. 4. Magnitude plots according to detection point 1, series and parallel models and comparison with experimental values for tap water.

(a) Impedance series arrangement, see Fig. 2(a), $H_s(\alpha = 0)$.
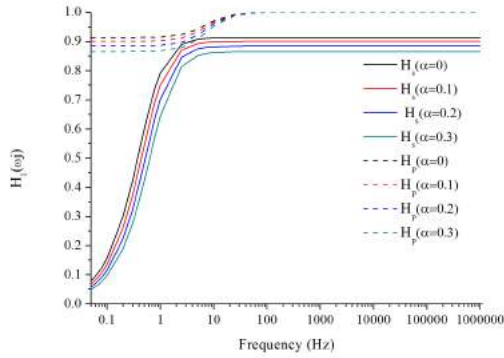

(b) Impedance parallel arrangement, see Fig. 2(b), $H_p(\alpha = 0)$.

Fig. 5. Magnitude plots according to detection point 2 and comparison with experimental values for tap water.

point 2 (see Fig. 5). A horizontal slope is also shown by the parallel model in point 1 (Fig. 4) but its magnitude does not fit the experimental values. In the detection point 2 above 1 *kHz*, the series model fits experimental values (see Fig. 5), while the parallel model holds a negative slope, even from 10 *Hz*, performing as a capacitive element.

Nevertheless, as frequency becomes smaller, experimental data in detection point 1 (see Fig. 4) are better fitted by the series model, as compared to the parallel one. Below 10 *Hz*, experimental data exhibits an inductive behavior and the series model also presents an inductive pattern up to 1 *Hz*, fitting experimental points, even if fitting is not as accurate as in the resistive range. In this interval the parallel model holds a resistive pattern that cannot fit the data, the adjustment of both models to the experimental data was intent for values of $R_z = 95\,\Omega$ and $C_z = 250\,\mu F$. These values were chosen for further studies on the series and parallel transfer functions, even when void fractions are different from zero. Below 10 *Hz*, better

adjustment to data should be expected by including a parasitic capacitance or a polarization resistance, as a third element. While this approach could give a better fitting, it does not contribute to the comparison of the models proposed here and should be considered by further studies.

4.3 Void Fraction modelling

The two-phase resistance and capacitance, given by Eqs. (6) and (7), respectively, were substituted into the transfer functions, Eqs. (10) and (11), for detection point 1, as well as in the transfer functions, Eqs. (12) and (13), for detection point 2, for proposed constant parametric values of $\alpha = \{0.0, 0.1, 0.2, 0.3\}$. This set of α values embraces the bubbly flow pattern in bubble columns. Results are shown in Fig. 6(a) for the detection point 1 and in Fig. 6(b) for the detection point 2.

(a) Impedance series arrangement, see Fig. 2(a), $H_s(\alpha = 0)$.
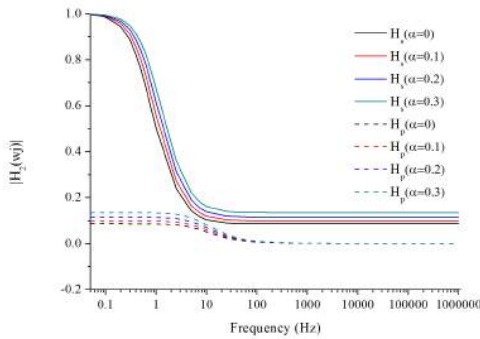
(b) Impedance parallel arrangement, see Fig. 2(b), $H_p(\alpha = 0)$.

Fig. 6. Magnitude plots for series and parallel models for proposed parametric values of $\alpha = \{0.0, 0.1, 0.2, 0.3\}$.

One of the most relevant features to be noticed in both Figs. 6(a) and 6(b) is that the parallel model is insensitive to changes in volume fraction at frequencies higher than 100 Hz. Thus, the parallel model is only capable to discriminate the void fraction at excitation frequencies below 10 Hz, where reactive behavior becomes relevant and polarization of electrodes is to be considered important. However, it is also in this range of excitation frequencies that the parallel model presents lack of fitting, as shown above, in Figs. 4 and 5. Therefore, the parallel model does not fit the experimental behavior at low frequencies and is insensitive to void fraction at high frequencies. Both drawbacks are fixed by the series model.

Conclusions

The comparison of the series model and the parallel model for a basic circuit composed just by a resistor and a capacitor, as the primary elements of an electrical system arranged by a set of plates flushed on the wall of a cylindrical pipe filled with tap water, gave rise to the following conclusions:

1. The series model presents a resistive behavior at excitation frequencies above $1\,kHz$. It also presents an inductive behavior at point 1 for frequencies between $0.1\,Hz$ and $1\,Hz$, and a capacitive behavior at point 2 between $0.3\,Hz$ and $3\,Hz$. These facts are consistent with experimental results for tap water.

2. At point 1 the parallel model presents a resistive behavior at frequencies below $1\,Hz$ and a second resistive behavior above $10\,Hz$. There is also an inductive behavior between these frequencies. At point 2 the behavior is resistive at frequencies smaller than $1\,Hz$ and capacitive with very small magnitudes above $1\,kHz$. This behavior was made apparent by using the *dB* scale.

3. Below $10\,Hz$ an inductive experimental behavior is observed at point 1. This behavior follows the general trend predicted by the series model and cannot be fitted by the parallel model. Moreover, below $1\,Hz$ the parallel model presents a resistive behavior that is not consistent with experimental observations.

4. Above $1\,kHz$ a resistive experimental behavior at point 2 is observed. This behavior is fitted by the series model and is not fitted by the parallel one which hold a capacitive behavior with very small magnitude.

5. While the parallel model presents insensitivity to the gas volume fraction at higher frequencies than $100\,Hz$, the series model is sensitive to changes in computed volume fraction. This is an important point to be accounted for in further studies on void fraction measurement capabilities, since sensor calibrations may introduce theoretical expressions for two-phase electrical parameters, *i.e.* Eqs. (6) and (7), into appropriate electrode modelling, in order to account for the gas volume fraction, as we suggest here.

6. The series model should be extended by considering a further element, probably a parasitic capacitance or a polarization resistance. Nevertheless, the most important features of the experimental behavior, both at low and at high frequencies, are well represented by the simple series model discussed here.

Acknowledgments

Nomenclature

C_{TP} two phase capacitance
C_z water capacitance
H transfer function
j imaginary number unit
R resistance
R_{TP} two phase resistance
R_z water resistance
V_{in} voltage feed
V_k voltage at point k, for k=1, 2
Z electrical impedance
Greek symbols
α void fraction
ω angular frequency

References

Banasiak, R., Wajman, R., Jaworski, T., Fiderek, P., Fidos, H., Nowakowski, J., Sankowski, D. (2014) Study on two-phase flow regime visualization and identification using 3D electrical capacitance tomography and fuzzy logic classification. *International Journal of Multiphase Flow 58*, 1-14.

Bernier, R.J. (1982). Unsteady two-phase flow instrumentation and measurement. Ph.D. Thesis, Doctor of Philosophy, California Institute of Technology, Pasadena, California.

Cheng H., Hills J.H., Azzopardi B.J. (2002) Effects of initial bubble size on flow pattern transition in a 28.9 mm diameter column. *International Journal of Multiphase Flow 28*, 10473-10620.

Costigan G., Whalley P.B. (1997). Slung flow regime identification from dynamic void fraction measurement in vertical air - water flows. *Int. J. Multiphase Flow 23*, 263-282.

Coutinho, F.R., Ofuchi, C.Y., de Arruda, L.V.R., Jr., F.N., Morales, R.E.M. (2014). A New Method for Ultrasound Detection of Interfacial Position in Gas-Liquid Two-Phase Flow. *Sensors 14*, 9093-9116.

Devia, F., Fossa, M. (2003). Design and optimization of impedance probes for void fraction measurements. *Flow Measurement and Instrumentation 14*, 139-149.

dos Reis, E., da Silva, C.D. (2014). Experimental study on different configurations of capacitive sensors for measuring the volumetric concentration in two-phase flows. *Flow Measurement and Instrumentation 37*, 127-134.

Falcone, G. (2009a). Multiphase Flow Fundamentals, In: *Developments in Petroleum Science*, (G. Falcone, G.F. Hewitt, C. Alimonti, eds), Elsevier, 54:1-18.

Falcone, G. (2009b). Key Multiphase Flow Metering Techniques, In: *Developments in Petroleum Science*. (G. Falcone, G.F. Hewitt, C. Alimonti, eds), Elsevier, 54:47-190.

George, D. L., Torczynski, J., Shollenberger, K., O'Hern, T., Ceccio, S. (2001) Three-phase material distribution measurements in a vertical flow using gamma-densitometry tomography and electrical-impedance tomography. *International Journal of Multiphase Flow 27*, 1903-1930.

Jaworek, A., Krupa, A., Trela, M. (2004). Capacitance sensor for void fraction measurement in water/steam flows. *Flow Measurement and Instrumentation 15*, 317-324.

Ko, M.S., Lee, B.A., Won, W. Y., Lee, Y.G., Jerng, D.W., Kim, S. (2015). An improved electrical-conductance sensor for void-fraction measurement in a horizontal pipe. *Nuclear Engineering and Technology 47*, 804-813.

Kytömaa, H.K., Brennen, C.E.(1988) Some observations of flow patterns and statistical properties of three component flow. *Journal of Fluids Engineering 110*, 76-84.

Li, H., Ji, H., Huang, Z., Wang, B., Li, H., Wu, G. (2016). A New Void Fraction Measurement Method for Gas-Liquid Two-Phase Flow in Small Channels. *Sensors 16*, 159.

Mansfeld, F., Shih, H., Greene, H., and Tsai, C. H. (1993). Analysis of EIS Data for Common Corrosion Processes, In: *Electrochemical Impedance: Analysis and Interpretation*, (J.R. Scully, D.C. Silverman, and M.W. Kendig,

eds.), American Society for Testing and Materials, Philadelphia, 37-53.

Martínez Gómez, R., Soria, A. (2003). An application of finite elements to the design of electrical impedance tomography systems. *Revista Mexicana de Ingeniería Química 2*, 127-133.

Micaelli, J.C. (1982). Propagation d'ondes dans les écoulements diphasiques á bulles á deux constituants. Étude théorique et expérimentale. Ph.D. Thèse, L'Institut National Polytechnique, Grenoble.

Prasser, H.M., (2007). Evolution of interfacial area concentration in a vertical air-water flow measured by wire-mesh sensors. *Nuclear Engineering and Design 237*, 1608-1617.

Rocha, M.S., Simões-Moreira, J.R. (2008). Void Fraction Measurement and Signal Analysis from Multiple-Electrode Impedance Sensors, *Heat Transfer Engineering 29*, 924-935.

Rodríguez, J.C. (2006). Pressure waves in a bubble column, Master Thesis (in Spanish), Master Degree, Universidad Autónoma Metropolitana-Iztapalapa, Mexico City.

Saiz-Jabardo, J.M., Bouré, J.A. (1988). Experiments on void fraction waves. *International Journal of Multiphase Flow 15*, 483-493.

Sánchez-López, J.R.G., Soria, A., Salinas-Rodríguez, E. (2011) Compressible and Incompressible 1-D Linear Wave Propagation Assessment in Fast Fluidized Beds. *AIChE Journal 57*, 2965-2976.

Song, C.H., No H.C., Chung M.K. (1995). Investigation of bubble flow developments and its transition based on the instability of void fraction waves. *International Journal od Multiphase Flow 21*,381-404.

Soria, A., Salinas-Rodríguez, E. (2013) Assessing Significant Phenomena in Linear Perturbation Multiphase Flows. In: *Fluid Dynamics in Physics, Engineering and Environmental Applications* (Klapp J., Medina A., Cross A., Vargas C.A., eds), Springer-Verlag, 93-110.

Spedding, P., Nguyen, V. (1980). Regime maps for air-water two-phase flow. *Chemical Engineering Science 35*, 779-793.

Taitel, Y., Bornea, D., Dukler, A. (1980). Modeling flow pattern transitions for steady upward gas-liquid flow in vertical tubes. *AIChE Journal 26*, 345-354.

Tournaire, A. (1986). Dependence of the instantaneous response of impedance probes on the local distribution of the void fraction in a pipe. *International Journal of Multiphase Flow 12*, 1019-1024.

Tournaire, A. (1987). Détection et étude des ondes de taux de vide en écoulements diphasique a bulles jusqu'a la transition bulles-bouchons. Ph.D. Thèse. L'Institut National Polytechnique, Grenoble.

Tri, B.D. (2005). Identification of two phase flow regimes by void fraction measurements. *Vietnam Journal of Mechanics 27*, 59-65.

Wu, H., Tan, C., Dong, X., Dong, F. (2015). Design of a Conductance and Capacitance Combination Sensor for water hold up measurement in oil-water two-phase flow. *Flow Measurement and Instrumentation 46*, 218-229.

Yang, H., Kim, D., Kim, M. (2003). Void fraction measurement using impedance method. *Flow Measurement and Instrumentation 14*, 151-160.

Zenit, R., Hunt, M.L. (2000) Solid fraction fluctuations in solid-liquid flows. *International Journal of Multiphase Flow 26*, 763-781.